HHS Public Access

Author manuscript

J Mol Biol. Author manuscript; available in PMC 2021 September 04.

Published in final edited form as:

J Mol Biol. 2020 September 04; 432(19): 5287–5303. doi:10.1016/j.jmb.2020.07.014.

Highly conserved molecular features in IgLONs contrast their distinct structural and biological outcomes

Harikanth Venkannagari[1,2,#], **James M. Kasper**[1,3,#], **Anurag Misra**[1,2,#], **Scott A. Rush**[1,2], **Shanghua Fan**[1,2], **Hubert Lee**[1,2], **Hong Sun**[1,3], **Suchithra Seshadrinathan**[1,2], **Mischa Machius**[1,2], **Jonathan D. Hommel**[1,3], **Gabby Rudenko**[1,2,3,*]

[1]Dept. of Pharmacology and Toxicology; University of Texas Medical Branch, Galveston, TX, USA

[2]Sealy Center for Structural Biology and Molecular Biophysics; University of Texas Medical Branch, Galveston, TX, USA

[3]Center for Addiction Research; University of Texas Medical Branch, Galveston, TX, USA

Abstract

Neuronal growth regulator 1 (NEGR1) and neurotrimin (NTM) are abundant cell-surface proteins found in brain and form part of the IgLON (Immunoglobulin LSAMP, OBCAM, Neurotrimin) family. In humans, NEGR1 is implicated in obesity and mental disorders, while NTM is linked to intelligence and cognitive function. IgLONs dimerize homophilically and heterophilically, and they are thought to shape synaptic connections and neural circuits by acting *in trans* (spanning cellular junctions) and/or *in cis* (at the same side of a junction). Here, we reveal homodimeric structures of NEGR1 and NTM. They assemble into V-shaped complexes via their Ig1 domains, and disruption of the Ig1-Ig1 interface abolishes dimerization in solution. A hydrophobic ridge from one Ig1 domain inserts into a hydrophobic pocket from the opposing Ig1 domain producing an interaction interface that is highly conserved among IgLONs but remarkably plastic structurally. Given the high degree of sequence conservation at the interaction interface, we tested whether different IgLONs could elicit the same biological effect *in vivo*. In a small scale study, administering different soluble IgLONs directly into the brain and monitoring feeding, only NEGR1 altered food intake significantly. Taking NEGR1 as a prototype, our studies thus indicate that while IgLONs share a conserved mode of interaction and are able to bind each other as homomers and heteromers, they are structurally plastic and can exert unique biological action.

[*]Correspondence: G. Rudenko, Dept. Pharmacology/Toxicology, and the Sealy Center for Structural Biology, University of Texas Medical Branch, 301 University Blvd. Galveston, TX 77555, USA, garudenk@utmb.edu.

Author Contributions:

GR and JH supervised the project; HV, HL, SR, and SS performed molecular biology, protein purification and/or crystallization. HV carried out the analytical ultracentrifugation studies. SF and HL carried out surface plasmon resonance studies. MM, HV, AM, and SR carried out data collection, data processing, structure determinations, and/or the structural analyses. JK and HS carried out animal studies and immunohistochemistry. All authors contributed to the manuscript.

[#]co-first authors;

Accession Numbers: Atomic coordinates and structure factors for the NEGR1 and NTM homodimeric crystal structures are deposited in the Protein Data Bank (PDB IDs: 6U6T and 6U7N, respectively).

Graphical Abstract

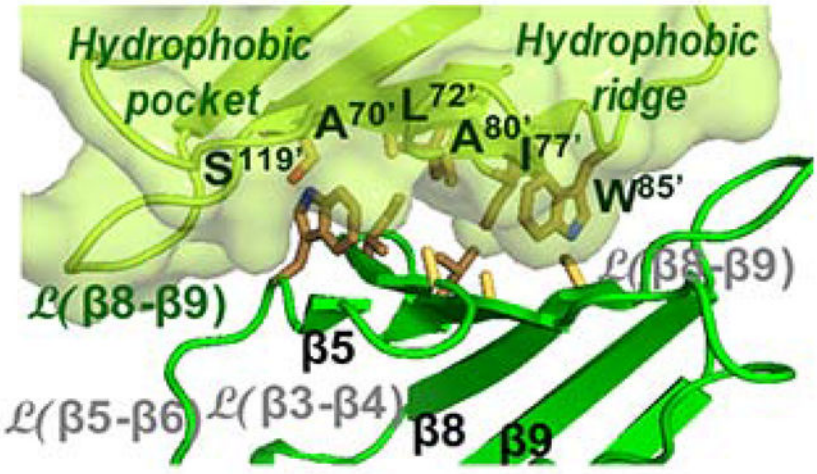

Keywords

IgLONs; synaptic organizer; protein structure; obesity; neuropsychiatric disorders

Introduction

The IgLON family of synaptic adhesion molecules comprises neuronal growth regulator 1 (NEGR1/IgLON4), neurotrimin (NTM/IgLON2), opioid binding protein/cell adhesion molecule-like (OPCML/OBCAM/IgLON1), limbic system associated membrane protein (LSAMP/IgLON3), and IGLON5. IgLONs are composed of three Ig domains and are anchored to the membrane by a glycosylphosphatidylinositol (GPI) moiety [1]. They are found on the surface of neurons and oligodendrocytes, except for NTM, which is restricted to neurons [2]. Perhaps the best studied, NEGR1 localizes to post-synaptic sites of dendritic and somatic synapses [2–5]. NEGR1 is involved in promoting neurite outgrowth, the migration of neurons to their target brain region, spine formation, dendritic tree formation and adult neurogenesis [6–12]. Similarly, NTM, LSAMP, and OBCAM increase and/or decrease neuron adhesion, neurite outgrowth, and synapse formation as well, though their roles are less well characterized [13–15].

IgLONs protrude into the synaptic cleft where they recruit partners. NEGR1 and NTM interact both homophilically as well as heterophilically, and bind *in trans* (spanning the synaptic cleft) and *in cis* (on the same membrane) [4,6,10,12,14,16–20]. Recently, leukemia inhibitory factor receptor (LIFR), fibroblast growth factor receptor 2 (FGFR2), and Niemann-Pick disease type C protein (NPC2) have been reported to bind NEGR1 as well [7,12,21]. Soluble IgLONs may have biological functions as well because NEGR1 and NTM ectodomains are also shed from the cell surface via metalloproteases, an alternative splice form of NTM lacking its GPI anchor is secreted, and soluble NEGR1 promotes neurite outgrowth [8,22,23].

IgLONs are implicated in a number of diseases. Single-nucleotide polymorphisms (SNPs) and copy-number variations (CNVs) implicate NEGR1 in obesity and possibly bulimia [24–32]. NEGR1 is also linked to Major Depressive Disorder (MDD) as well as schizophrenia (SZ), dyslexia, autism spectrum disorder (ASD), cognitive disabilities, and lower white matter integrity across the brain [12,33–35]. By contrast, NTM is linked to intelligence and cognitive function [36]; LSAMP to mood disorders [11,37] and heart disease [38]; OBCAM, a tumor-suppressor [1], to cognitive deficits [39]; and IgLON5 to encephalopathy, sleep dysfunction, chronic neurodegeneration, and auto-immune disorders [40].

The underlying molecular mechanisms of IgLON function are not well understood. Here, we report crystal structures of homodimers of NEGR1 and NTM, two IgLONs that are of particular interest because they modulate neural circuits impacting feeding, emotions, social behavior, and cognition. Together with recent crystal structures of other IgLONs, the complete body of structural work now permits a cohesive analysis of IgLON complexes revealing a general mechanism of interaction that is highly conserved but remarkably plastic structurally. Based on these insights, we also tested different IgLONs *in vivo* for their biological activity and the importance of homo- and/or heterodimer formation. We administered IgLON ectodomains into the paraventricular nucleus of the hypothalamus (PVN), a brain region that is a critical regulator of feeding [41–43]. Only NEGR1 altered food intake while other IgLONs did not, and interestingly, an intact IgLON binding site was not required for this activity. Together, our data suggest novel structure-function relationships for the IgLON family.

Results

The crystal structure of NEGR1 was determined using X-ray diffraction data to a resolution of 3.01 Å (Table 1; Fig. S1). The NEGR1 monomer contains three Ig domains in a linear concatenation (Fig. 1a; Fig. S2). The molecule is rigidified by two long, continuous β-strands (β9 and β15) that work as connectors integrating into the β-sandwiches from two adjacent Ig domains (Ig1-Ig2, and Ig2-Ig3, respectively). Each of the three Ig domains belongs to a different Ig-fold subtype whereby Ig1 is a V-type Ig domain, Ig2 adopts a C2 type and Ig3 an I type (Fig. 1b) (classified according to [44]). We also determined the crystal structure of NTM using X-ray diffraction data to a resolution of 3.32 Å (Table 1). Like NEGR1, NTM reveals a linear array of three Ig domains rigidified by two long β-strands (β9 and β15) (Fig. 2a; Fig. S3) and contains a V-type Ig1, a C2-type Ig2, but a C1-type Ig3 (Fig. 2b).

With the exception of LSAMP, there are now crystal structures available for all homomeric IgLONs: NEGR1 (reported here), NTM (reported here, and also in [20] referred to here as NTM*), OBCAM (PDB ID: 5UV6), and IgLON5 [20], though the latter only at medium resolution; as well as for the NEGR1/IgLON5 heterodimer [20]. Critical comparison of these structures allows the identification of shared as well as divergent features and sheds light onto how IgLONs may assemble at cellular junctions. While the Ig1, Ig2, and Ig3 domains contain different Ig-fold subtypes, they maintain a very high degree of structural similarity (Fig. 3a). The Ig2 domains are the most similar (rmsd = 0.45 Å for 82 out of ~85 C^{α} atoms) with only one loop, L(β12-β12'), being highly variable (Fig. 3a). By contrast, Ig1

and Ig3 contain several loops located at the outer ends of the molecules that are highly divergent (loops L(β2-β3), L(β6-β7), and L(β8-β9) in Ig1 and loops L(β15-β16), L(β17-β17'), L(β17'-β18) and L(β19-β20) in Ig3, respectively), though the cores of these domains are very similar (Ig1: rmsd = 0.62 Å for 87 out of 91 C^{α} atoms; Ig3: rmsd = 0.74 Å for 81 out of ~86 C^{α} atoms) (Fig. 3a). The ectodomains bend to variable extents in the different homomer structures (Fig. 3b).

NEGR1 and NTM share a common mode of interaction that involves the Ig1 domains from two monomers contacting each other to form V-shaped homodimers (Fig. 4a; Fig. S4). The Ig1-Ig1 interface buries between 720 $Å^2$ solvent accessible surface per monomer in NEGR1 and about 850 $Å^2$ in NTM, respectively (Fig. S4). The paired Ig1-Ig1 'headpieces' are generally structurally similar between the different IgLONs (Fig. 4b), but they exhibit an unexpected breadth of relative rotations and translations, even between NTM and NTM* (though these structures were determined under different crystallization conditions in different space groups). One consequence of this variability is that the V-shaped dimers are splayed apart to varying degrees in the different structures (Fig. 4c).

The IgLON interaction interface is formed mainly by a concave surface generated by β-strands β3, β4, β5, and β8 of the inner β-sheet and residues from the loops that connect these strands (Fig. 5a). The opposing Ig1 domain packs against this surface like a palm-to-palm handshake, that is, with the interacting β-sheets stacked but rotated by about 90 degrees with respect to each other (Fig. 5a). The majority of the interactions at the Ig1-Ig1 interface are hydrophobic in nature (Fig. 5b; Fig. 5c). At the core of the interaction surface lies a hydrophobic pocket lined by atoms from six conserved, small residues (the side chains of Ala^{70}, Ala^{80}, and Ser^{119}, as well as the main chains of Gly^{81}, Gly^{69}, and Val^{120}; residue numbers are that in NEGR1; see Table 2 for equivalent residues in the other IgLON structures). On one side, this pocket is flanked by a hydrophobic ridge containing three adjacent conserved residues: a leucine, an interleaved isoleucine, and a tryptophan (Leu^{72}; Ile^{77}; and Trp^{85} in NEGR1). On the other side, a wall is formed by loop L(β8-β9) (Gln^{121}–Pro^{126} in NEGR1) (Fig. 5a). The residues and their interactions at the interface are qualitatively highly conserved across the IgLON structures, but there are characteristic spatial differences (Fig. 5d; Fig. 5e; Table 2; Fig. S5). The strictly conserved tryptophan of the hydrophobic ridge (Trp^{85}NEGR1) is uniquely situated to facilitate varying relative dispositions of the Ig1 domains within the IgLON dimers (Fig. 4b; Fig. 4c). This Trp inserts into the hydrophobic pocket in the opposing Ig1 domain upon dimerization, like a peg into a hole (Fig. 5e). In addition to the residues lining the pocket, the Trp peg also packs against side chains from loop L(β2-β3) (Lys^{68}NEGR1) and from loop L(β8-β9) (Gln^{121}NEGR1) (Fig. 5b; Fig. 5c). Despite being completely buried deep in the interface, the Trp peg adopts dramatically different rotamer conformations, even in structures of the same proteins (e.g., in NTM and NTM*, as well as in NEGR1 in the NEGR1/IgLON5 heterodimer) indicating structural plasticity (Fig. 5e; S6; S7). The periphery of the interface, however, is less conserved. For example, loop L(β8-β9) has limited sequence conservation and molds into different conformations at the dimerization interface in the different IgLONs, suggesting that it might steer selectivity (Fig. 5d; Table 2). Nevertheless, regardless of the structural plasticity observed at the Ig1-Ig1 interface, the sequence conservation here remains very

high, especially when contrasted, for example, against the backside of the Ig1 domain (Fig. 5f).

We next probed IgLON interaction biophysically. We tested the binding affinity of NEGR1 to different IgLONs using surface plasmon resonance (SPR). In keeping with the high level of conservation observed at the Ig1-Ig1 interface, NEGR1 binds to different IgLONs with very similar affinity (K_D ~ 21 – 42 nM) (Fig. 6). To probe the importance of key residues at the Ig1-Ig1 interface, we generated IgLON mutants and determined their oligomeric status in solution by analytical ultracentrifugation. Establishing a baseline, sedimentation velocity experiments of wild-type proteins show that in the range of 10–20 μM, NEGR1, NTM, OBCAM, and LSAMP form homogenous species with $S_{20,w}$ values of 3.7–4.0 (Fig. 7a; Fig. S8). At 20 μM, estimated molecular weights are 59–82 kDa, i.e. approximately twice the theoretical molecular weight of 31.9–32.4 kDa (based on amino acid sequence), indicating that these proteins are dimeric in solution. It is important to point out that the derivation of these molecular weights does not take into account the heavy glycosylation (Fig. S8a) for the calculation of partial specific volumes, making it also difficult to reliably carry out further modeling studies to investigate the state of the molecules. We then generated, based on the structural information, mutants with the aim of disrupting the Ig1-Ig1 interface of NEGR1. And indeed, the four NEGR1 mutants generated, $A^{70}D$, $W^{85}A$, $A^{70}D/W^{85}A$, and $I^{77}A/A^{80}D/W^{85}A$ each give species with an $S_{20,w}$ ~2.6–2.7 corresponding to particles with molecular weights of 30–37 kDa, indicating that they are present as monomers in solution (Fig. 7b).

Intrigued by the striking sequence conservation of the Ig1-Ig1 interface and the conserved mode of interaction among IgLONs, yet different attributed biological roles, we administered IgLON ectodomains into the paraventricular nucleus of the hypothalamus (PVN) and monitored acute changes in food intake, given the robust genetic link between NEGR1 and obesity as well as body mass index. The PVN has a well-documented role in regulating food intake [41–46] so that NEGR1 ectodomains administered to the PVN should competitively bind to endogenous binding sites and impact feeding. Though limited in scope, these studies show that only NEGR1 alters food intake in rats when administered *in vivo* to the PVN (a decrease of ~20% compared to the vehicle aCSF) while other IgLONs do not (Fig. S8; Fig. S9a-f), and a dose as low as 1 pmole is sufficient to induce a decrease in food intake (Fig. S9g-h) presumably by blocking endogenous binding sites (Fig. S9i-j) and does not lead to gross behavioral abnormalities (Fig. S9k-l). Furthermore, NEGR1 does not require an intact IgLON binding site for this activity because dimerization defect mutants, NEGR1 $W^{85}A$ and NEGR1 $A^{70}D$, also decrease food consumption similarly compared to vehicle (Fig. S9m-n). Thus despite a conserved IgLON binding mechanism, NEGR1 uniquely decreases food intake when administered to the PVN, and dimerization of NEGR1 is not required for this activity.

Discussion

Here, we reveal detailed structure-function relationships for the IgLON family, rod-like ectodomains that assemble into V-shaped dimers via interaction of their Ig1 domains. The highly conserved Ig1-Ig1 interaction site is characterized by a hydrophobic ridge from one

monomer packing against a largely hydrophobic depression on the opposing monomer. Structural plasticity allows the two Ig1 domains in the different IgLON dimers to assemble with varying relative dispositions. Strikingly, despite the conserved nature of the Ig1-Ig1 interactions, only the ectodomain of NEGR1 and its dimerization deficient mutants show biological activity in a feeding-based *in vivo* assay.

The assembly of IgLONs via their Ig1 domain resembles that seen for the 11-member DIP and 21-member DPR families of cell adhesion molecules [47]. In the DIP/DPR system, subtle structural differences are thought to lead to specific homophilic and/or heterophilic dimeric complexes that help establish specific visual circuits in drosophila and that display binding affinities in the range of 1–200 μM [48–50]. By contrast, IgLONs bind each other with nanomolar affinities (here and in [20]). The DIP/DPR dimerization interfaces are much flatter compared to IgLONs and do not contain a pronounced hydrophobic ridge (Fig. 8a; Fig. 8b). Interestingly, DIP residues located in the loop that is equivalent to L(β3-β4) in IgLONs insert between loops in DPR that are equivalent to L(β3-β4) and L(β8-β9) of the partnering IgLONs; these loops feature high sequence variability and contain residues that confer selectivity between DIP/DPR combinations [48], lending support to the notion that loop L(β8-β9) in IgLONs may also steer selective interactions between specific IgLON family members.

IgLONs are reported to interact both *in trans* and *in cis* [6,10,12], but their exact localization at synapses remains to be determined. For example, NEGR1 and LSAMP localize to postsynaptic sites [3–5,51], but their presence on presynaptic membranes is unclear, and thus how they are incorporated at synapses as well. Synaptic clefts in the CNS span ~200–240 Å at excitatory synapses [52–55] and ~120 Å at inhibitory synapses [56], though narrower gaps have been suggested for excitatory (~160 Å) and inhibitory (~100 Å) synapses, respectively [56]. The NEGR1 ectodomain is ~124 Å x 52 Å x 32 Å and an additional ~12 residues tether it to the GPI anchor embedded in the synaptic membrane (Fig. 8c). The dimensions of NTM are very similar (~124 Å x 45 Å x 35 Å). As a V-shaped homodimer, the NEGR1 dimer spans ~200 Å and is ~77 Å x 39 Å wide (NTM spans ~195 Å x 71 Å x 46 Å). Thus, even though the V-shaped dimer can flex somewhat, its outer ends that tether it to one or two membranes still span close to 200 Å (Fig. 8c). As such, an IgLON dimer would readily fit *in trans* spanning the synaptic cleft at excitatory synapses (Fig. 8c). Alternatively, dimeric complexes of IgLONs could readily be tethered *in cis* to a single (post-synaptic) membrane and bind other pre-synaptic partners as well (Fig. 8c). Therefore, future studies will be needed to determine exactly where IgLONs are located within synapses, and whether these complexes are tethered *in trans* or *in cis*.

To probe structure-function relationships, we administered IgLONs into the PVN and monitored the effect on food intake as a proxy for biological activity. Genetic lesions link NEGR1 robustly to altered body mass index and obesity in humans [6,27,29–32,57,58]. NEGR1, but not other IgLONs, altered feeding (Fig. S9), even though they are all expressed in the hypothalamus [1] and they share a highly conserved Ig1-Ig1 interaction surface (Fig. 8d). In support, genome-wide association studies have so far only implicated NEGR1, and not other IgLONs, in altered body mass index and obesity. Interestingly, the decrease in food intake observed following NEGR1 administration (> 20%) is similar to that seen following

treatment with lorcaserin, a weight loss drug [59] and its potency is in the range of the well-characterized feeding peptide MTII, a melanocortin-4 receptor agonist [60,61]. Our observation that NEGR1 interface mutants also elicit a similar biological response as wild type NEGR1 (Fig. S9m-n) suggests that dimerization is not essential for all its biological roles and/or that other partners may be involved. Hence, an important future line of research will be to determine the primary partners for NEGR1 that support its different biological functions and unique roles in different neural circuits. Our results suggest new models for IgLON function. IgLONs are typically thought of as trans-synaptic adhesion molecules forming homodimers or heterodimers that span the synaptic cleft (Fig. 8c) [1]. For instance, neuronal migration, dendritic formation, and synapse development in neural circuit formation have been attributed to cell adhesion mediated by IgLONs [6–12]. Our data support a model whereby binding to non-IgLON partners may be an important component of NEGR1's biological role as well, e.g., LIFR binds NEGR1 independent of the Ig1 domain [7]. This further suggests that surfaces outside the highly conserved Ig1-Ig1 interface (Fig. 8d) are also important and form binding sites for non-IgLON protein partners. Mapping of the sequence conservation between NEGR1s and NTMs (the latter does not alter food intake in our studies), reveals marked differences between them, for example, on the 'backside' of Ig1 and Ig3, potentially indicating binding sites for partners that uniquely interact with different IgLONs (Fig. 8e). By contrast, NEGR1 and NTM, each, are virtually completely conserved within mammals (Fig. 8f). Therefore, the current models of IgLON structure-function relationships are likely incomplete and should be extended beyond a simple *trans*-synaptic IgLON adhesion model (Fig. 8c).

Materials and Methods

Protein expression and purification:

The extracellular domains of NEGR1 (Q7Z3B1, a.a. 38–313), NTM (Q9P121, a.a. 36–311), OBCAM (Q14982, a.a. 36–312), LSAMP (Q13449, a.a. 32–306) and mutants of the NEGR1 ectodomain ($A^{70}D$, $W^{85}A$, $I^{77}A/A^{80}D/W^{85}A$, and $A^{70}D/W^{85}A$) with a C-terminal linker and hexahistidine ('His')-tag were cloned into the pFastbac vector. Also, hemagglutinin (HA)-tagged NEGR1 containing a C-terminal HA-tag followed by a TEV cleavage site (GENLYFQG) and a His-tag were cloned into the pFastbac vector as well. All proteins were expressed in HighFive cells using the baculovirus mediated expression system. Cells were grown in Excel 405 serum free medium (Sigma, St. Louis, MO) with additional L-glutamine and antibiotics/antimycotics added, with an infection course of 72–80 hr. After infection, the medium containing the secreted proteins was collected, protease inhibitors (PMSF, pepstatin, and leupeptin) added, then concentrated and dialyzed overnight into 25 mM sodium phosphate pH 8.0, 500 mM NaCl. After dialysis, proteins were purified using Ni-NTA affinity chromatography. The purified His-tagged proteins were dialyzed into 25 mM Tris pH 8.0, 50 mM NaCl and further purified by ion-exchange chromatography (Mono Q; GE Healthcare, Chicago, IL). Finally, all the proteins were purified by size exclusion chromatography (HiLoad Superdex-200 16/600 or HiLoad Superdex-75 16/600; GE Healthcare, Chicago, IL) in 10 mM HEPES pH 8.0, 150 mM NaCl. Purified proteins were concentrated to 2.5–7.5 mg/ml and stored at −80 °C by flash-freezing aliquots in liquid nitrogen. For the HA-NEGR1 protein, after Ni-NTA affinity chromatography and ion-

exchange chromatography, the His-tag was removed by adding His-tagged TEV enzyme (1:30 molar ratio). To facilitate the proteolytic activity, the reaction was performed in a redox component buffer consisting of 25 mM Tris pH 8, 500 mM NaCl, 0.3 mM oxidized glutathione and 0.3 mM reduced glutathione, overnight at 4°C. Subsequently, uncut NEGR1 with the His-tag still intact and the His-tagged TEV was removed by flowing the reaction mixture over a 1 ml HisTrap HP Ni-NTA column (GE healthcare). HA-NEGR1 was collected in the flow-through and removal of the His-tag was validated by western blot analysis using an anti-His-tag antibody. The final purified HA-NEGR1 protein was buffer exchanged into 10 mM HEPES pH 8.0, 150 mM NaCl, concentrated to 1.9 mg/ml, aliquoted and flash frozen in liquid nitrogen.

Crystallization:

Crystals of NEGR1 were grown at 20 °C by mixing 1 μl of protein (2.5 mg/ml) and 1 μl of reservoir solution (20% (w/v) PEG 3350, 0.1 M Tris pH 9.0, 0.2 M $MgCl_2$, 0.6 M NaI) in a hanging drop setup. Single crystals were obtained via microseeding, and their size improved to ~600 × 200 μm by macroseeding. Crystals harvested from the crystallization drops were cryo-protected in reservoir solution containing 20% (v/v) MPD and then flash cooled by plunging into liquid nitrogen. The crystals exhibit the symmetry of space group $C222_1$ with unit cell dimensions of a=73.57 Å, b=97.24 Å, c=252.41 Å, α=β=γ=90° and diffracted to ca. 3.0 Å. Crystals of NTM were obtained by mixing 2 μl of protein (5.4 mg/ml) and 2 μl of reservoir solution (2.5 M NaCl, 100 mM sodium acetate pH 4.5, 200 mM Li_2SO_4) in a hanging drop setup and incubating at 20 °C. Single crystals with a size of ~250 × 150 μm were obtained in 7–10 days. Crystals harvested from the crystallization drops were cryo-protected in reservoir solution containing 20% (v/v) ethylene glycol and then flash cooled by plunging into liquid nitrogen. The crystals exhibit the symmetry of space group I4 with unit cell dimensions of a=b=106.05 Å, c=227.81 Å, α=β=γ=90° and diffracted to ca. 3.3 Å. Diffraction datasets were collected at the Advanced Photon Source (LS-CAT, SBC-CAT and IMCA-CAT). Data were processed using HKL2000 [62] and data statistics are given in Table 1.

Structure Determination of NEGR1 and NTM:

The structures of NEGR1 and NTM were determined by molecular replacement with PHASER [63] using the coordinates of OBCAM (PDB ID: 5UV6) as a search model. Model building was done using Coot [64] in an iterative manner interspersed with refinement using PHENIX [65]. Because of the relatively low resolution of the diffraction data, further confounded by anisotropic diffraction, the geometry of the models was tightly restrained using automatic X-ray/geometry weighting routines in Phenix, resulting in relatively small deviations in bond lengths and bond angles from ideal geometry. The refined model for NEGR1 consists of 542 residues with good geometry: 96.1% residues in the favored region, 3.9% in the allowed region, and one outliers in the Ramachandran plot (Arg74 in both molecules in the asymmetric unit), two calcium ions, six N-acetyl glucosamines (NAG), three β-D-mannose (BMA), and two fucose (FUC) molecules. The N-terminal 14 and 11 residues, respectively, in the two molecules in the asymmetric unit and the C-terminal 10 residues in both molecules in the asymmetric unit were not included in the model due to lack of corresponding electron density. The refined model for NTM consists of 256 residues with

good geometry: 94.8% in the favored region, 5.2% in the allowed region, and no outliers in the Ramachandran plot, three NAG, one BMA, and one FUC molecule as well as three ethylene glycol (EDO) molecules, and 4 chloride ions. The N-terminal 38 residues, residues 231 to 239, and the C-terminal 8 residues were not included in the model due to lack of corresponding electron density. Hydrogen atoms were added to the riding positions of all models in refinements. Ligands modeled in the structures were validated in omit maps (Fig. S1).

Structure analysis:

Secondary structure analysis was done using Stride [66]. Buried surface analysis of NEGR1, NTM, and OBCAM was performed using ePISA [67]. Superpositions were carried out using the 'gesamt' program [68] from the CCP4 suite [69] with the coordinates for OBCAM (PDB ID: 5UV6), IgLON5 (PDB ID: 6DLE), and the IgLON5/NEGR1 heterocomplex (PDB ID: 6DLD). Interactions between IgLONs were assessed using NCONT in CCP4 [69] to identify distances less than 5 Å. Sequence alignments were performed using Clustal Omega [70] and displayed using ESPript [71]. Sequence homology comparisons were carried out with the following sequences (UniProt codes): NEGR1 (human, Q7Z3B1; rat, Q9Z0J8; mouse, Q80Z24), NTM (human, Q9P121; bovine, A0A3S5HJV5; rat, Q62718, mouse, Q99PJ0), OBCAM (human, Q99PJ0), LSAMP (human, Q13449; IgLON5 (human, A6NGN9), DIPη (Q9VMN9) and DPR1 (Q8T603). Residue conservation is as defined in Clustal Omega [70]. Figures were prepared using the PyMol Molecular Graphics System, Schrödinger, LLC.

Surface Plasmon Resonance:

Binding of IgLONs to NEGR1 was assessed in Running Buffer (10 mM HEPES pH 7.4, 150 mM NaCl and 0.05% (v/v) Surfactant P20) at 25°C on a Biacore T100 SPR instrument. NEGR1 was immobilized on a CM5 sensor chip (5540.4 RU; GE Healthcare). Specific binding data was obtained by injecting soluble ectodomains of NEGR1-$(His)_6$, LSAMP-$(His)_6$, NTM-$(His)_6$ and OBCAM-$(His)_6$ in a concentration series over the NEGR1-coupled sensor, corrected by subtraction of the signal collected simultaneously from flowing IgLONs over the sensor with no ligand immobilized. The following IgLON concentrations were used: (0, 12.5, 25.0, 50.0, 100.0 nM) flowed at 30 μl/min for 120 s (association step) followed by Running Buffer for 120 s (dissociation step). The sensor was regenerated after each protein injection with 5 mM NaOH. The data was processed using a kinetic analysis and the K_D calculated from sensorgram data fit to a 1:1 stoichiometric bimolecular association model. The curves were fit using Rmax local fitting. The K_D values for NEGR1 binding to different IgLONs were calculated by averaging two independent experiments (the average and error (standard deviation) are shown).

Analytical Ultracentrifugation:

The solution oligomerization state of different IgLONs (NEGR1, NTM, OBCAM, and LSAMP) and mutants of NEGR1 was analyzed by the Sedimentation Velocity (SV) method. All experiments were performed using a Beckman Optima XL-1 analytical ultracentrifuge (Beckman Coulter, Indianapolis, IN) equipped with an absorbance detection system and an An60 Ti rotor at 42,000 rpm (141,995 RCF) at a temperature of 4 °C. SV experiments were performed using 12-mm double sector (2-channel) charcoal-filled epon centerpieces

enclosed with quartz windows. Proteins were dialyzed at 4 °C for four hours against a ~1000-fold volume of buffer (10 mM HEPES pH 8.0, 100 mM NaCl). Dialysis buffer was also used as the reference solution. Three different concentrations of NEGR1, NTM, OBCAM and LSAMP were analyzed (10 μM, 15 μM, and 20 μM). NEGR1 mutants were analyzed at 10 μM only. SV data were analyzed with SEDFIT version 14.81 [72], using the continuous sedimentation coefficient distribution model $c(s)$ to calculate the distribution and sedimentation coefficients of the sedimenting species. Partial specific volumes for proteins, viscosity and density for buffers were calculated using SEDNTERP [73]. We accounted for the time- and radius-invariant noise, and maximum-entropy regularization of the $c(s)$ model was set to a confidence level of 0.65. Standardization of S values ($s_{20,w}$) and generation of high resolution plots were performed using Gussi 1.0.8 [74]. Predicted molecular weights (M_w) for the recombinant proteins based on their amino acid sequences are for NEGR1 31,863.8 Da, NTM 32,136.1 Da, OBCAM 32,401.5 Da, and LSAMP 32,165.7 Da; in addition, all four proteins are extensively N-linked glycosylated.

Animal studies:

Male Sprague-Dawley rats (Harlan Laboratories, Indianapolis, IN) weighing 225–250 grams were used for all immunostaining and feeding experiments. Rats were allowed to habituate in the colony room for one week after arrival before all experiments. Separate cohorts of rats were used for each study. Experiments were carried out in accordance with the Guide for the Care and Use of Laboratory Animals and with the approval of the Institutional Animal Care and Use Committee at the University of Texas Medical Branch.

Immunostaining:

Rats (N=3) were euthanized, perfused with 4% paraformaldehyde, and brain tissue was collected for immunohistochemistry as previously described [75,76]. Briefly, 40 μm thick brain slices were washed 3 times for 5 minutes each with 1x PBS, antigen unmasked for 5 minutes in 1% SDS, washed again, and blocked for 1 hour in 3% normal mouse serum and 0.3% Triton X-100 in 1x PBS. Tissue was then incubated with 25 μg HA-NEGR1 ectodomain in 1 ml blocking solution for 3 days at 4°C. Subsequently, the tissue was washed 3 times as before, and incubated in a 1:200 dilution of anti-HA-tag Dylight 550 antibody (26183-D550, Invitrogen) in 1x PBS for 2 hours. Tissue was then washed again, mounted, and coverslipped with DPX. Images were taken on a Leica TCS SPE confocal DMI4000 inverted microscope with a 5x or 40x objective of tissue with or without HA-NEGR1 incubation, followed by incubation with the anti-HA-tag antibody. Images were pseudo-colored green for interpretation and publication.

Feeding studies:

Rats were single housed in their home cage and maintained on a diet of normal chow (Teklad LM-485 Mouse/Rat Sterilizable Diet; Teklad Diets) which was available to rats during all feeding studies. Rats (n=48) underwent stereotaxic surgery as previously described [75] and were implanted with bilateral guide cannula (C309GA, Small Parts) directed 2 mm above the PVN (anterior/posterior −1.8 mm, medial/lateral +1.5 mm, dorsal/ventral −6.2 mm from bregma) [46]. Rats were allowed to recover for 1 week and were habituated to daily handling. Three days before experimental testing, rats were exposed to a

highly palatable 45% fat diet (Open Source Diets formula D12451, Research Diets Inc.) by placing 30 gr of this diet into the home cage. Following this pre-exposure, the rats only had access to this highly palatable diet during experimental tests, while regular chow remained available at all times. Rats were separated into three cohorts, one for the multiple IgLON comparisons and locomotor activity, one for the NEGR1 dose effect study, and one for studies with NEGR1 mutants. Over the course of two weeks, each rat received single acute doses of NEGR1, NTM, LSAMP, OBCAM ectodomains (10 pmoles) or aCSF. After each administration, the rats were exposed to highly palatable food for 4 hours and the amount of the food ingested monitored. This experimental paradigm was chosen to determine the immediate biological effects that IgLON administration might have, before the onset of long-term, in-direct effects. Each study employed a Latin square design for IgLON administration whereby rats received each of the IgLONs or vehicle in a random order of treatment. This design minimizes the effect of inter-animal feeding variability on collected data. A 2–3 day ‘washout’ period was included between each IgLON administration. This washout allowed animals to return to baseline feeding behavior because no significant lingering effects were observed during vehicle treatment, suggesting the treatment effects are reversible. OBCAM was also administered in parallel, but removed from the studies, when within 24 hours after administration, 3 of 4 animals expired with no obvious signs of the cause of death, even though no clear signs of distress were noted for up to 4 hours following administration of OBCAM. Feeding studies for highly palatable food were conducted 4 hours after the start of the light phase of the light/dark cycle; the light phase is well suited to avoid ‘binge’ consumption that takes place at the start of the dark cycle [77]. IgLONs were diluted to the given concentrations in artificial cerebrospinal fluid and 1.2 μl of solution was administered bilaterally (0.6 μl per side) through the guide cannula into the PVN of the non-anesthetized rats, a volume that is guided by our previous studies and the spread of the injections into the rat PVN [46]. Rats were immediately placed back in their home cage with an additional food hopper containing highly palatable food, and intake of this food was monitored for 4 hours. A 4-hour window was long enough to measure meaningful differences in food intake. The difference in weight of the hopper before and after 4 hours represents the food consumed by the rat following intra-PVN IgLON administration. Following the study, rats were euthanized and targeting of the guide cannula was confirmed. Rats with misplaced cannula, clogged cannula, or signs of infection were excluded from study (total n=14). Data were analyzed using within subjects oneway ANOVA and post hoc test or t-test using the Prism version 6 software.

Supplementary Material

Refer to Web version on PubMed Central for supplementary material.

Acknowledgements:

This work is funded by NIMH (R01MH077303), NIDDK (R01DK106229), and the Sealy Center for Structural Biology and Molecular Biophysics (SCSB) at UTMB. The Advanced Photon Source (LS-CAT, SBC-CAT and IMCA-CAT) are thanked for access to synchrotron radiation and assistance during data collection, Drs. Mark White and Luis Holthauzen at the SCSB for helpful discussions, and Fang Chen for preliminary studies. Dr. Chad Brautigam at the University of Texas Southwestern Medical Center is gratefully acknowledged for extensive discussions regarding the processing of analytical ultracentrifugation data.

Abbreviations:

3D	three dimensional
AAV	adeno-associated virus
ASD	autism spectrum disorder
CNS	central nervous system
F_c region	fragment crystallizable region of an antibody
FGFR2	fibroblast growth factor receptor 2
GPI	glycosylphosphatidylinositol
Ig	immunoglobulin
IgLON family	immunoglobulin LSAMP, OBCAM, and Neurotrimin family
LIFR	leukemia inhibitory factor receptor
MDD	major depressive disorder
NPC2	Niemann-Pick type C2 protein
PVN	paraventricular nucleus of the hypothalamus
rmsd	root mean square deviation
SEM	standard deviation of the mean
SZ	schizophrenia

REFERENCES

[1]. Vanaveski T, Singh K, Narvik J, Eskla K-L, Visnapuu T, Heinla I, Jayaram M, Innos J, Lilleväli K, Philips M-A, Vasar E, Promoter-Specific Expression and Genomic Structure of IgLON Family Genes in Mouse, Front. Neurosci. 11 (2017). 10.3389/fnins.2017.00038.

[2]. Sharma K, Schmitt S, Bergner CG, Tyanova S, Kannaiyan N, Manrique-Hoyos N, Kongi K, Cantuti L, Hanisch U-K, Philips M-A, Rossner MJ, Mann M, Simons M, Cell type- and brain region-resolved mouse brain proteome, Nat. Neurosci 18 (2015) 1819–1831. 10.1038/nn.4160. [PubMed: 26523646]

[3]. Funatsu N, Miyata S, Kumanogoh H, Shigeta M, Hamada K, Endo Y, Sokawa Y, Maekawa S, Characterization of a novel rat brain glycosylphosphatidylinositol-anchored protein (Kilon), a member of the IgLON cell adhesion molecule family, J. Biol. Chem 274 (1999) 8224–8230. [PubMed: 10075727]

[4]. Miyata S, Matsumoto N, Taguchi K, Akagi A, Iino T, Funatsu N, Maekawa S, Biochemical and ultrastructural analyses of IgLON cell adhesion molecules, Kilon and OBCAM in the rat brain, Neuroscience. 117 (2003) 645–658. [PubMed: 12617969]

[5]. Struyk AF, Canoll PD, Wolfgang MJ, Rosen CL, D'Eustachio P, Salzer JL, Cloning of neurotrimin defines a new subfamily of differentially expressed neural cell adhesion molecules, J. Neurosci. Off. J. Soc. Neurosci 15 (1995) 2141–2156.

[6]. Lee AWS, Hengstler H, Schwald K, Berriel-Diaz M, Loreth D, Kirsch M, Kretz O, Haas CA, de Angelis MH, Herzig S, Brümmendorf T, Klingenspor M, Rathjen FG, Rozman J, Nicholson G, Cox RD, Schäfer MKE, Functional Inactivation of the Genome-Wide Association Study Obesity Gene Neuronal Growth Regulator 1 in Mice Causes a Body Mass Phenotype, PLOS ONE. 7 (2012) e41537 10.1371/journal.pone.0041537. [PubMed: 22844493]

[7]. Noh K, Lee H, Choi T-Y, Joo Y, Kim S-J, Kim H, Kim JY, Jahng JW, Lee S, Choi S-Y, Lee SJ, Negr1 controls adult hippocampal neurogenesis and affective behaviors, Mol. Psychiatry 24 (2019) 1189–1205. 10.1038/s41380-018-0347-3. [PubMed: 30651602]

[8]. Pischedda F, Piccoli G, The IgLON Family Member Negr1 Promotes Neuronal Arborization Acting as Soluble Factor via FGFR2, Front. Mol. Neurosci 8 (2015) 89 10.3389/fnmol.2015.00089. [PubMed: 26793057]

[9]. Pischedda F, Szczurkowska J, Cirnaru MD, Giesert F, Vezzoli E, Ueffing M, Sala C, Francolini M, Hauck SM, Cancedda L, Piccoli G, A cell surface biotinylation assay to reveal membrane-associated neuronal cues: Negr1 regulates dendritic arborization, Mol. Cell. Proteomics MCP 13 (2014) 733–748. 10.1074/mcp.M113.031716. [PubMed: 24382801]

[10]. Reed J, McNamee C, Rackstraw S, Jenkins J, Moss D, Diglons are heterodimeric proteins composed of IgLON subunits, and Diglon-CO inhibits neurite outgrowth from cerebellar granule cells, J. Cell Sci 117 (2004) 3961–3973. 10.1242/jcs.01261. [PubMed: 15265982]

[11]. Singh K, Lilleväli K, Gilbert SF, Bregin A, Narvik J, Jayaram M, Rahi M, Innos J, Kaasik A, Vasar E, Philips M-A, The combined impact of IgLON family proteins Lsamp and Neurotrimin on developing neurons and behavioral profiles in mouse, Brain Res. Bull 140 (2018) 5–18. 10.1016/j.brainresbull.2018.03.013. [PubMed: 29605488]

[12]. Szczurkowska J, Pischedda F, Pinto B, Managò F, Haas CA, Summa M, Bertorelli R, Papaleo F, Schäfer MK, Piccoli G, Cancedda L, NEGR1 and FGFR2 cooperatively regulate cortical development and core behaviours related to autism disorders in mice, Brain J. Neurol 141 (2018) 2772–2794. 10.1093/brain/awy190.

[13]. Akeel M, McNamee CJ, Youssef S, Moss D, DIgLONs inhibit initiation of neurite outgrowth from forebrain neurons via an IgLON-containing receptor complex, Brain Res. 1374 (2011) 27–35. 10.1016/j.brainres.2010.12.028. [PubMed: 21167820]

[14]. Gil OD, Zhang L, Chen S, Ren YQ, Pimenta A, Zanazzi G, Hillman D, Levitt P, Salzer JL, Complementary expression and heterophilic interactions between IgLON family members neurotrimin and LAMP, J. Neurobiol 51 (2002) 190–204. 10.1002/neu.10050. [PubMed: 11984841]

[15]. Hashimoto T, Maekawa S, Miyata S, IgLON cell adhesion molecules regulate synaptogenesis in hippocampal neurons, Cell Biochem. Funct 27 (2009) 496–498. 10.1002/cbf.1600. [PubMed: 19711485]

[16]. Cheng S, Park Y, Kurleto JD, Jeon M, Zinn K, Thornton JW, Özkan E, Family of neural wiring receptors in bilaterians defined by phylogenetic, biochemical, and structural evidence, Proc. Natl. Acad. Sci. U. S. A 116 (2019) 9837–9842. 10.1073/pnas.1818631116. [PubMed: 31043568]

[17]. Gil OD, Zanazzi G, Struyk AF, Salzer JL, Neurotrimin mediates bifunctional effects on neurite outgrowth via homophilic and heterophilic interactions, J. Neurosci. Off. J. Soc. Neurosci 18 (1998) 9312–9325.

[18]. Lodge AP, Howard MR, McNamee CJ, Moss DJ, Co-localisation, heterophilic interactions and regulated expression of IgLON family proteins in the chick nervous system, Brain Res. Mol. Brain Res 82 (2000) 84–94. [PubMed: 11042360]

[19]. McNamee CJ, Reed JE, Howard MR, Lodge AP, Moss DJ, Promotion of neuronal cell adhesion by members of the IgLON family occurs in the absence of either support or modification of neurite outgrowth, J. Neurochem 80 (2002) 941–948. 10.1046/j.0022-3042.2002.00798.x. [PubMed: 11953444]

[20]. Ranaivoson FM, Turk LS, Ozgul S, Kakehi S, von Daake S, Lopez N, Trobiani L, De Jaco A, Denissova N, Demeler B, Özkan E, Montelione GT, Comoletti D, A Proteomic Screen of Neuronal Cell-Surface Molecules Reveals IgLONs as Structurally Conserved Interaction Modules at the Synapse, Struct. Lond. Engl. 1993 27 (2019) 893–906.e9. 10.1016/j.str.2019.03.004.

[21]. Kim H, Chun Y, Che L, Kim J, Lee S, Lee S, The new obesity-associated protein, neuronal growth regulator 1 (NEGR1), is implicated in Niemann-Pick disease Type C (NPC2)-mediated cholesterol trafficking, Biochem. Biophys. Res. Commun 482 (2017) 1367–1374. 10.1016/j.bbrc.2016.12.043. [PubMed: 27940359]

[22]. Lodge AP, McNamee CJ, Howard MR, Reed JE, Moss DJ, Identification and characterization of CEPU-Se-A secreted isoform of the IgLON family protein, CEPU-1, Mol. Cell. Neurosci 17 (2001) 746–760. 10.1006/mcne.2001.0964. [PubMed: 11312609]

[23]. Sanz R, Ferraro GB, Fournier AE, IgLON cell adhesion molecules are shed from the cell surface of cortical neurons to promote neuronal growth, J. Biol. Chem 290 (2015) 4330–4342. 10.1074/jbc.M114.628438. [PubMed: 25538237]

[24]. Delahanty LM, Pan Q, Jablonski KA, Watson KE, McCaffery JM, Shuldiner A, Kahn SE, Knowler WC, Florez JC, Franks PW, Diabetes Prevention Program Research Group, Genetic predictors of weight loss and weight regain after intensive lifestyle modification, metformin treatment, or standard care in the Diabetes Prevention Program, Diabetes Care. 35 (2012) 363–366. 10.2337/dc11-1328. [PubMed: 22179955]

[25]. Fox CS, Liu Y, White CC, Feitosa M, Smith AV, Heard-Costa N, Lohman K, Consortium G, Consortium M, Consortium G, Johnson AD, Foster MC, Greenawalt DM, Griffin P, Ding J, Newman AB, Tylavsky F, Miljkovic I, Kritchevsky SB, Launer L, Garcia M, Eiriksdottir G, Carr JJ, Gudnason V, Harris TB, Cupples LA, Borecki IB, Genome-Wide Association for Abdominal Subcutaneous and Visceral Adipose Reveals a Novel Locus for Visceral Fat in Women, PLOS Genet. 8 (2012) e1002695 10.1371/journal.pgen.1002695. [PubMed: 22589738]

[26]. Gamero-Villarroel C, González LM, Gordillo I, Carrillo JA, García-Herráiz A, Flores I, Rodríguez-López R, Gervasini G, Impact of NEGR1 genetic variability on psychological traits of patients with eating disorders, Pharmacogenomics J. 15 (2015) 278–283. 10.1038/tpj.2014.53. [PubMed: 25245582]

[27]. Jarick I, Vogel CIG, Scherag S, Schäfer H, Hebebrand J, Hinney A, Scherag A, Novel common copy number variation for early onset extreme obesity on chromosome 11q11 identified by a genome-wide analysis, Hum. Mol. Genet 20 (2011) 840–852. 10.1093/hmg/ddq518. [PubMed: 21131291]

[28]. Mägi R, Manning S, Yousseif A, Pucci A, Santini F, Karra E, Querci G, Pelosini C, McCarthy MI, Lindgren CM, Batterham RL, Contribution of 32 GWAS-identified common variants to severe obesity in European adults referred for bariatric surgery, PloS One. 8 (2013) e70735 10.1371/journal.pone.0070735. [PubMed: 23950990]

[29]. Speliotes EK, et al., Association analyses of 249,796 individuals reveal 18 new loci associated with body mass index, Nat. Genet 42 (2010) 937–948. 10.1038/ng.686. [PubMed: 20935630]

[30]. Thorleifsson G, Walters GB, Gudbjartsson DF, Steinthorsdottir V, Sulem P, Helgadottir A, Styrkarsdottir U, Gretarsdottir S, Thorlacius S, Jonsdottir I, Jonsdottir T, Olafsdottir EJ, Olafsdottir GH, Jonsson T, Jonsson F, Borch-Johnsen K, Hansen T, Andersen G, Jorgensen T, Lauritzen T, Aben KK, Verbeek AL, Roeleveld N, Kampman E, Yanek LR, Becker LC, Tryggvadottir L, Rafnar T, Becker DM, Gulcher J, Kiemeney LA, Pedersen O, Kong A, Thorsteinsdottir U, Stefansson K, Genome-wide association yields new sequence variants at seven loci that associate with measures of obesity, Nat. Genet 41 (2009) 18–24. 10.1038/ng.274. [PubMed: 19079260]

[31]. Wheeler E, Huang N, Bochukova EG, Keogh JM, Lindsay S, Garg S, Henning E, Blackburn H, Loos RJF, Wareham NJ, O'Rahilly S, Hurles ME, Barroso I, Farooqi IS, Genome-wide SNP and CNV analysis identifies common and low-frequency variants associated with severe early-onset obesity, Nat. Genet 45 (2013) 513–517. 10.1038/ng.2607. [PubMed: 23563609]

[32]. Willer CJ, et al., Six new loci associated with body mass index highlight a neuronal influence on body weight regulation, Nat. Genet 41 (2009) 25–34. 10.1038/ng.287. [PubMed: 19079261]

[33]. Cross-Disorder Group of the Psychiatric Genomics Consortium, Genomic Relationships, Novel Loci, and Pleiotropic Mechanisms across Eight Psychiatric Disorders, Cell. 179 (2019) 1469–1482.e11. 10.1016/j.cell.2019.11.020. [PubMed: 31835028]

[34]. Dennis EL, Jahanshad N, Braskie MN, Warstadt NM, Hibar DP, Kohannim O, Nir TM, McMahon KL, de Zubicaray GI, Montgomery GW, Martin NG, Toga AW, Wright MJ, Thompson

PM, Obesity gene NEGR1 associated with white matter integrity in healthy young adults, NeuroImage. 102 Pt 2 (2014) 548–557. 10.1016/j.neuroimage.2014.07.041. [PubMed: 25072390]

[35]. Hyde CL, Nagle MW, Tian C, Chen X, Paciga SA, Wendland JR, Tung JY, Hinds DA, Perlis RH, Winslow AR, Identification of 15 genetic loci associated with risk of major depression in individuals of European descent, Nat. Genet 48 (2016) 1031–1036. 10.1038/ng.3623. [PubMed: 27479909]

[36]. Pan Y, Wang K-S, Aragam N, NTM and NR3C2 polymorphisms influencing intelligence: family-based association studies, Prog. Neuropsychopharmacol. Biol. Psychiatry 35 (2011) 154–160. 10.1016/j.pnpbp.2010.10.016. [PubMed: 21036197]

[37]. Innos J, Koido K, Philips M-A, Vasar E, Limbic system associated membrane protein as a potential target for neuropsychiatric disorders, Front. Pharmacol 4 (2013). 10.3389/fphar.2013.00032.

[38]. Wang L, Hauser ER, Shah SH, Seo D, Sivashanmugam P, Exum ST, Gregory SG, Granger CB, Haines JL, Jones CJH, Crossman D, Haynes C, Kraus WE, Freedman NJ, Pericak-Vance MA, Goldschmidt-Clermont PJ, Vance JM, Polymorphisms of the tumor suppressor gene LSAMP are associated with left main coronary artery disease, Ann. Hum. Genet 72 (2008) 443–453. 10.1111/j.1469-1809.2008.00433.x. [PubMed: 18318786]

[39]. Liu F, Arias-Vásquez A, Sleegers K, Aulchenko YS, Kayser M, Sanchez-Juan P, Feng B-J, Bertoli-Avella AM, van Swieten J, Axenovich TI, Heutink P, van Broeckhoven C, Oostra BA, van Duijn CM, A Genomewide Screen for Late-Onset Alzheimer Disease in a Genetically Isolated Dutch Population, Am. J. Hum. Genet 81 (2007) 17–31. 10.1086/518720. [PubMed: 17564960]

[40]. Dalmau J, Geis C, Graus F, Autoantibodies to Synaptic Receptors and Neuronal Cell Surface Proteins in Autoimmune Diseases of the Central Nervous System, Physiol. Rev 97 (2017) 839–887. 10.1152/physrev.00010.2016. [PubMed: 28298428]

[41]. Leibowitz SF, Hammer NJ, Chang K, Hypothalamic paraventricular nucleus lesions produce overeating and obesity in the rat, Physiol. Behav 27 (1981) 1031–1040. [PubMed: 7335803]

[42]. Miyata S, Funatsu N, Matsunaga W, Kiyohara T, Sokawa Y, Maekawa S, Expression of the IgLON cell adhesion molecules kilon and OBCAM in hypothalamic magnocellular neurons, J. Comp. Neurol 424 (2000) 74–85. 10.1002/1096-9861(20000814)424:1<74::AID-CNE6>3.0.CO;2-5. [PubMed: 10888740]

[43]. Morton GJ, Meek TH, Schwartz MW, Neurobiology of food intake in health and disease, Nat. Rev. Neurosci 15 (2014) 367–378. 10.1038/nrn3745. [PubMed: 24840801]

[44]. Bodelón G, Palomino C, Fernández LÁ, Immunoglobulin domains in Escherichia coli and other enterobacteria: from pathogenesis to applications in antibody technologies, FEMS Microbiol. Rev 37 (2013) 204–250. 10.1111/j.1574-6976.2012.00347.x. [PubMed: 22724448]

[45]. Benzon CR, Johnson SB, McCue DL, Li D, Green TA, Hommel JD, Neuromedin U receptor 2 knockdown in the paraventricular nucleus modifies behavioral responses to obesogenic high-fat food and leads to increased body weight, Neuroscience. 258 (2014) 270–279. 10.1016/j.neuroscience.2013.11.023. [PubMed: 24269937]

[46]. McCue DL, Kasper JM, Hommel JD, Regulation of motivation for food by neuromedin U in the paraventricular nucleus and the dorsal raphe nucleus, Int. J. Obes. 2005 41 (2017) 120–128. 10.1038/ijo.2016.178.

[47]. Aksu M, Seiradake E, DIPping into the Fly Visual System, Neuron. 100 (2018) 1270–1272. 10.1016/j.neuron.2018.11.044. [PubMed: 30571936]

[48]. Cosmanescu F, Katsamba PS, Sergeeva AP, Ahlsen G, Patel SD, Brewer JJ, Tan L, Xu S, Xiao Q, Nagarkar-Jaiswal S, Nern A, Bellen HJ, Zipursky SL, Honig B, Shapiro L, Neuron-Subtype-Specific Expression, Interaction Affinities, and Specificity Determinants of DIP/Dpr Cell Recognition Proteins, Neuron. 100 (2018) 1385–1400.e6. 10.1016/j.neuron.2018.10.046. [PubMed: 30467080]

[49]. Carrillo RA, Özkan E, Menon KP, Nagarkar-Jaiswal S, Lee P-T, Jeon M, Birnbaum ME, Bellen HJ, Garcia KC, Zinn K, Control of Synaptic Connectivity by a Network of Drosophila IgSF Cell Surface Proteins, Cell. 163 (2015) 1770–1782. 10.1016/j.cell.2015.11.022. [PubMed: 26687361]

[50]. Cheng S, Ashley J, Kurleto JD, Lobb-Rabe M, Park YJ, Carrillo RA, Özkan E, Molecular basis of synaptic specificity by immunoglobulin superfamily receptors in Drosophila, ELife. 8 (2019). 10.7554/eLife.41028.

[51]. Zacco A, Cooper V, Chantler PD, Fisher-Hyland S, Horton HL, Levitt P, Isolation, biochemical characterization and ultrastructural analysis of the limbic system-associated membrane protein (LAMP), a protein expressed by neurons comprising functional neural circuits, J. Neurosci. Off. J. Soc. Neurosci 10 (1990) 73–90.

[52]. de Arce KP, Schrod N, Metzbower SW, Allgeyer E, Kong GK-W, Tang A-H, Krupp AJ, Stein V, Liu X, Bewersdorf J, Topographic mapping of the synaptic cleft into adhesive nanodomains, Neuron. 88 (2015) 1165–1172. [PubMed: 26687224]

[53]. Harris KM, Weinberg RJ, Ultrastructure of synapses in the mammalian brain, Cold Spring Harb. Perspect. Biol. 4 (2012) a005587.

[54]. Lučic V, Yang T, Schweikert G, Förster F, Baumeister W, Morphological characterization of molecular complexes present in the synaptic cleft, Structure. 13 (2005) 423–434. [PubMed: 15766544]

[55]. Zuber B, Nikonenko I, Klauser P, Muller D, Dubochet J, The mammalian central nervous synaptic cleft contains a high density of periodically organized complexes, Proc. Natl. Acad. Sci. U. S. A 102 (2005) 19192–19197. [PubMed: 16354833]

[56]. High B, Cole AA, Chen X, Reese TS, Electron microscopic tomography reveals discrete transcleft elements at excitatory and inhibitory synapses, Front. Synaptic Neurosci 7 (2015) 9. [PubMed: 26113817]

[57]. Locke AE, et al., Genetic studies of body mass index yield new insights for obesity biology, Nature. 518 (2015) 197–206. 10.1038/nature14177. [PubMed: 25673413]

[58]. Tu W, Wagner EK, Eckert GJ, Yu Z, Hannon T, Pratt JH, He C, Associations between menarche-related genetic variants and pubertal growth in male and female adolescents, J. Adolesc. Health Off. Publ. Soc. Adolesc. Med 56 (2015) 66–72. 10.1016/j.jadohealth.2014.07.020.

[59]. Price AE, Brehm VD, Hommel JD, Anastasio NC, Cunningham KA, Pimavanserin and Lorcaserin Attenuate Measures of Binge Eating in Male Sprague-Dawley Rats, Front. Pharmacol 9 (2018) 1424 10.3389/fphar.2018.01424. [PubMed: 30581386]

[60]. Fan W, Boston BA, Kesterson RA, Hruby VJ, Cone RD, Role of melanocortinergic neurons in feeding and the agouti obesity syndrome, Nature. 385 (1997) 165–168. 10.1038/385165a0. [PubMed: 8990120]

[61]. Giraudo SQ, Billington CJ, Levine AS, Feeding effects of hypothalamic injection of melanocortin 4 receptor ligands, Brain Res. 809 (1998) 302–306. 10.1016/s0006-8993(98)00837-3. [PubMed: 9853124]

[62]. Otwinowski Z, Minor W, Processing of X-ray diffraction data collected in oscillation mode. Macromol Crystallogr A 276: 307–326, 1997.

[63]. McCoy AJ, Grosse-Kunstleve RW, Adams PD, Winn MD, Storoni LC, Read RJ, Phaser crystallographic software, J. Appl. Crystallogr 40 (2007) 658–674. [PubMed: 19461840]

[64]. Emsley P, Lohkamp B, Scott WG, Cowtan K, Features and development of Coot, Acta Crystallogr. D Biol. Crystallogr 66 (2010) 486–501. 10.1107/S0907444910007493. [PubMed: 20383002]

[65]. Adams PD, Afonine PV, Bunkóczi G, Chen VB, Davis IW, Echols N, Headd JJ, Hung L-W, Kapral GJ, Grosse-Kunstleve RW, McCoy AJ, Moriarty NW, Oeffner R, Read RJ, Richardson DC, Richardson JS, Terwilliger TC, Zwart PH, PHENIX: a comprehensive Python-based system for macromolecular structure solution, Acta Crystallogr. D Biol. Crystallogr 66 (2010) 213–221. 10.1107/S0907444909052925. [PubMed: 20124702]

[66]. Heinig M, Frishman D, STRIDE: a web server for secondary structure assignment from known atomic coordinates of proteins, Nucleic Acids Res. 32 (2004) W500–502. 10.1093/nar/gkh429. [PubMed: 15215436]

[67]. Krissinel E, Henrick K, Inference of macromolecular assemblies from crystalline state, J. Mol. Biol 372 (2007) 774–797. 10.1016/j.jmb.2007.05.022. [PubMed: 17681537]

[68]. Krissinel E, Enhanced fold recognition using efficient short fragment clustering, J. Mol. Biochem 1 (2012) 76–85. [PubMed: 27882309]

[69]. Winn MD, Ballard CC, Cowtan KD, Dodson EJ, Emsley P, Evans PR, Keegan RM, Krissinel EB, Leslie AG, McCoy A, Overview of the CCP4 suite and current developments, Acta Crystallogr. D Biol. Crystallogr 67 (2011) 235–242. [PubMed: 21460441]

[70]. Sievers F, Wilm A, Dineen D, Gibson TJ, Karplus K, Li W, Lopez R, McWilliam H, Remmert M, Söding J, Thompson JD, Higgins DG, Fast, scalable generation of high-quality protein multiple sequence alignments using Clustal Omega, Mol. Syst. Biol 7 (2011) 539 10.1038/msb.2011.75. [PubMed: 21988835]

[71]. Robert X, Gouet P, Deciphering key features in protein structures with the new ENDscript server, Nucleic Acids Res 42 (2014) W320–324. 10.1093/nar/gku316. [PubMed: 24753421]

[72]. Schuck P, Size-distribution analysis of macromolecules by sedimentation velocity ultracentrifugation and lamm equation modeling, Biophys. J 78 (2000) 1606–1619. 10.1016/S0006-3495(00)76713-0. [PubMed: 10692345]

[73]. Laue TM, Shah BD, Ridgeway TM, Pelletier SL, Analyticall Ultracentrifugation in Biochemistry and Polymer Science, in: Harding S, Rowe A (Eds.), Royal Society of Chemistry, 1992: pp. 90–125.

[74]. Brautigam CA, Chapter Five - Calculations and Publication-Quality Illustrations for Analytical Ultracentrifugation Data, in: Cole JL (Ed.), Methods Enzymol, Academic Press, 2015: pp. 109–133. 10.1016/bs.mie.2015.05.001.

[75]. Kasper JM, McCue DL, Milton AJ, Szwed A, Sampson CM, Huang M, Carlton S, Meltzer HY, Cunningham KA, Hommel JD, Gamma-Aminobutyric Acidergic Projections From the Dorsal Raphe to the Nucleus Accumbens Are Regulated by Neuromedin U, Biol. Psychiatry 80 (2016) 878–887. 10.1016/j.biopsych.2016.02.031. [PubMed: 27105831]

[76]. Smith AE, Kasper JM, Ara 13, Anastasio NC, Hommel JD, Binge-Type Eating in Rats is Facilitated by Neuromedin U Receptor 2 in the Nucleus Accumbens and Ventral Tegmental Area, Nutrients. 11 (2019). 10.3390/nu11020327.

[77]. Corwin RL, Avena NM, Boggiano MM, Feeding and reward: perspectives from three rat models of binge eating, Physiol. Behav 104 (2011) 87–97. 10.1016/j.physbeh.2011.04.041. [PubMed: 21549136]

Highlights

- The IgLONs, NEGR1 and NTM, organize protein networks in the synaptic cleft.
- The structures of NEGR1 and NTM reveal V-shaped dimers.
- The Ig1 domains host an interaction mechanism shared by IgLON homo- and heterodimers.
- NEGR1, implicated in obesity, regulates feeding in rats, unlike other IgLONs.
- The biological roles of IgLONs involve both shared and unique molecular features.

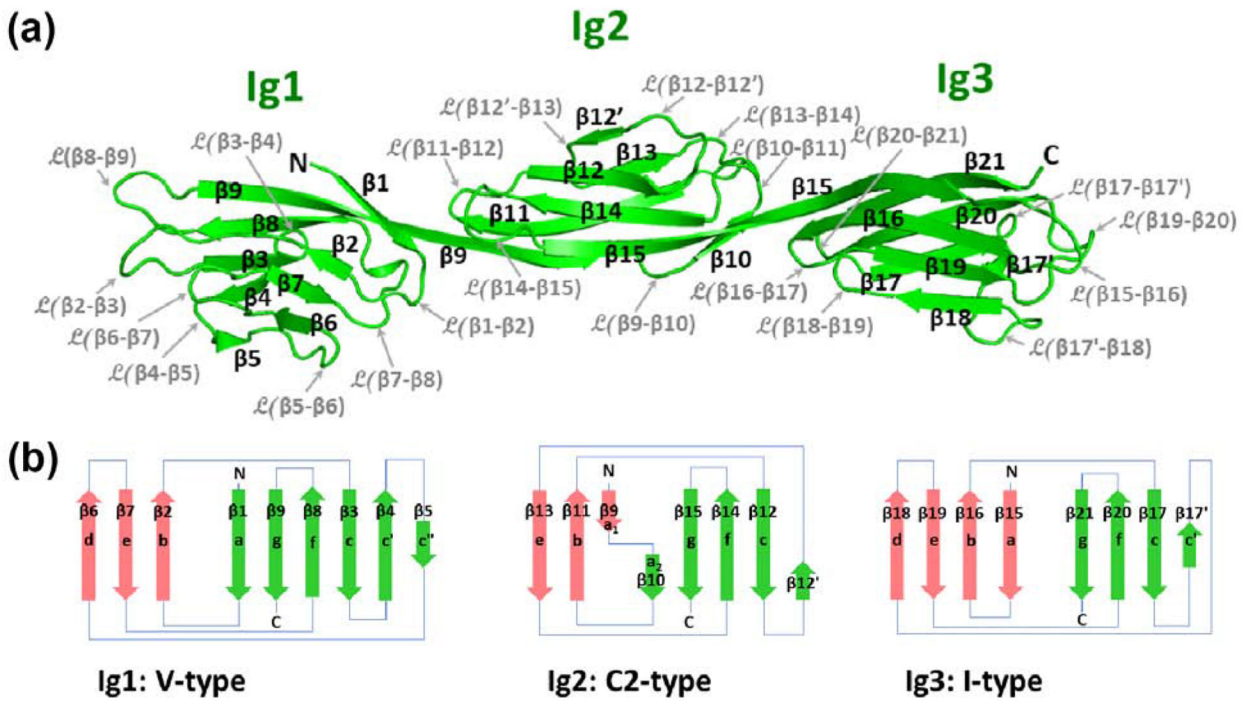

Figure 1: Crystal structure of NEGR1.

a) Cartoon representation of NEGR1. **b)** Topology diagram of the individual Ig domains.

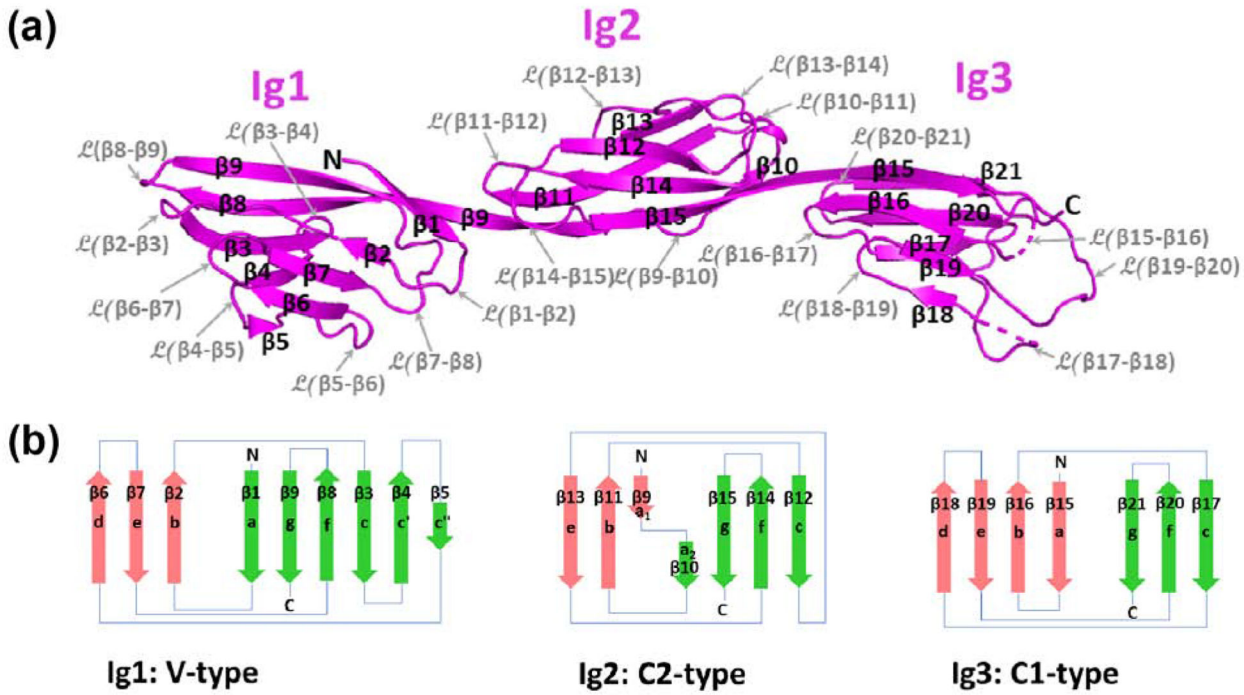

Figure 2: Crystal structure of NTM.

a) Cartoon representation of NTM. **b)** Topology diagram of the individual Ig domains.

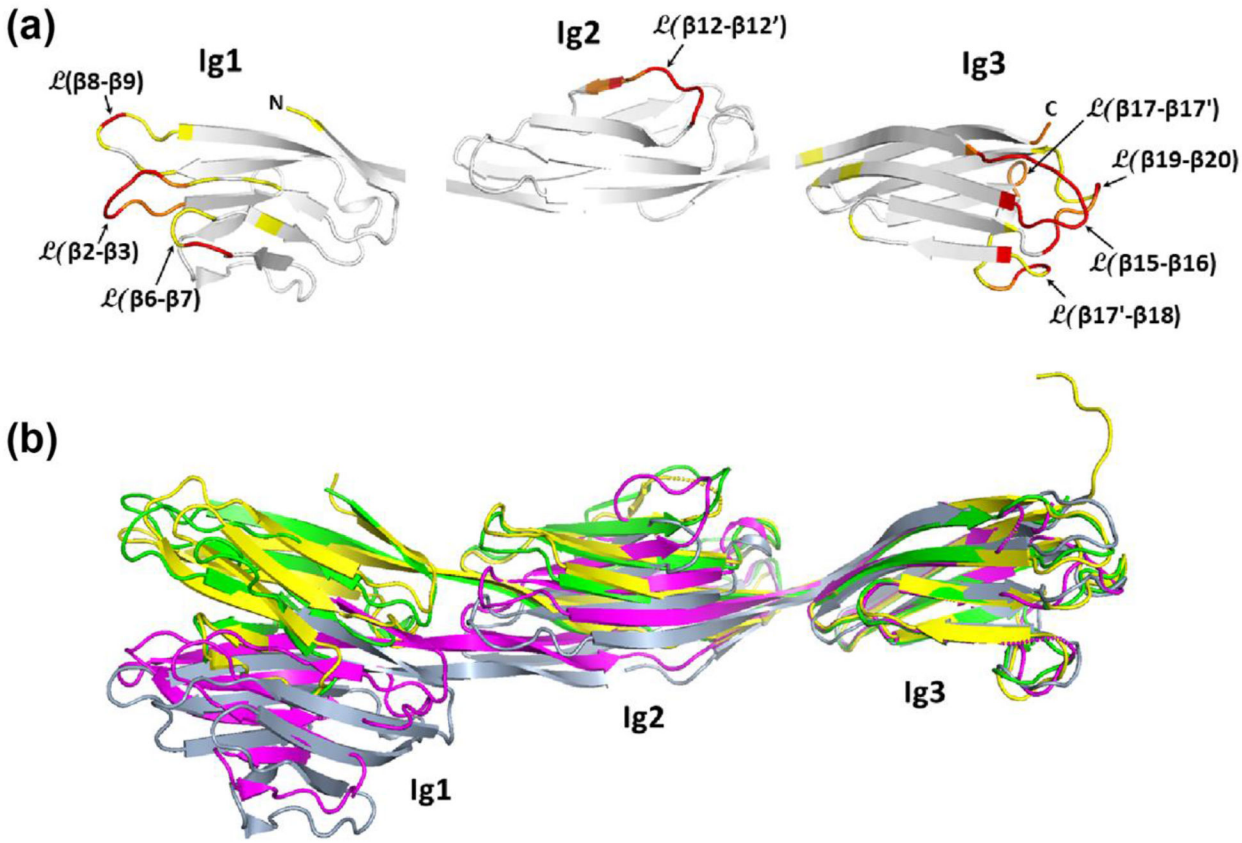

Figure 3: Superposition of IgLONs.

a) Structural variation between NEGR1, NTM, OBCAM, and IgLON5 ectodomains mapped onto the individual Ig domains of NEGR1 (white: rmsd 0.0–0.6 Å; yellow: rmsd 0.6–1.1 Å; orange: rmsd 1.1–2.0 Å; red: rmsd >2.0 Å). **b)** NEGR1 (green), NTM (magenta), OBCAM (yellow), and IGLON5 (blue-grey) monomers superimposed via their Ig3 domains showing an array of different ectodomain curvatures.

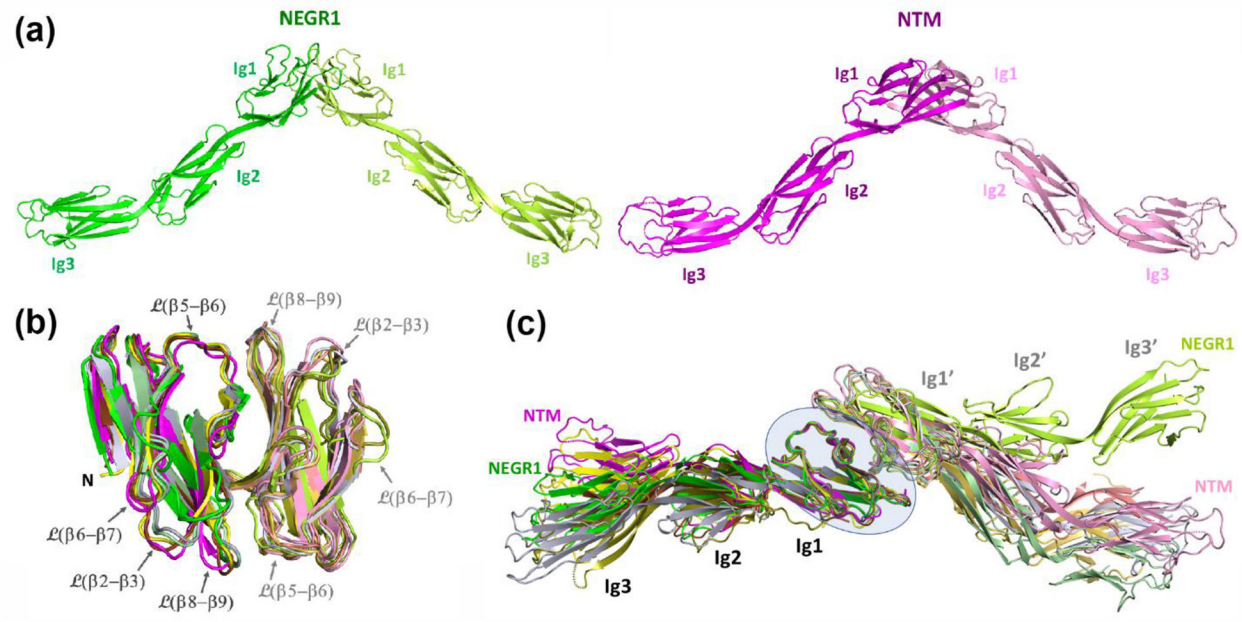

Figure 4: NEGR1 and NTM homodimers.

a) Homodimers of NEGR1 and NTM adopt a characteristic V-shaped structure. **b)** Superposition of the Ig1-Ig1 headpieces from homodimers of NEGR1 (green), NTM (magenta), NTM* (brown), OBCAM (yellow), IGLON5 (blue-grey), as well as an IGLON5/NEGR1 heterodimer (pale green/olive). Lighter and darker color palettes indicate the two individual Ig1 domains within the dimers. **c)** Superposition of the homodimers of NEGR1, NTM, NTM*, OBCAM, and IGLON5, and the IGLON5/NEGR1 heterodimer using Ig1. Colors as in **b)**.

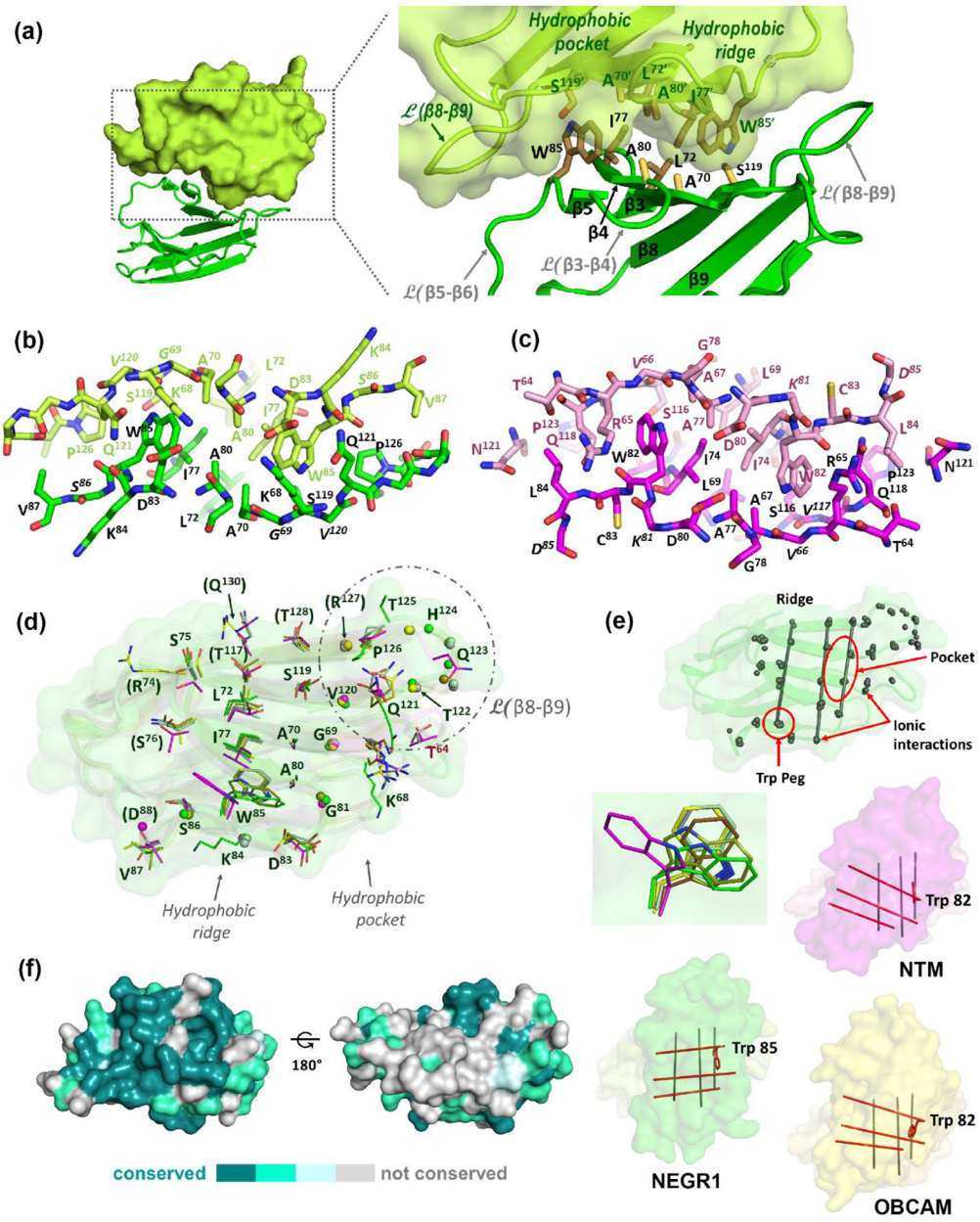

Figure 5: IgLON dimerization involves the Ig1-Ig1 interface.

a) The Ig1-Ig1 interface in NEGR1 involves a hydrophobic ridge (L^{72}, I^{77}, and W^{85}) docking against a hydrophobic pocket (A^{70}, A^{80}, S^{119}, G^{69}, G^{81}, V^{120}), and packing against a conformationally variable loop L(β8-β9). **b)** Close-up of the NEGR1 Ig1-Ig1 interface. Residues for which only the main chain is shown are in italics. **c)** Close-up of the NTM Ig1-Ig1 interface. Residues for which only the main chain is shown are in italics. **d)** Residues engaged in interactions across the Ig1-Ig1 interfaces of representative IgLONs (within 5 Å of their dimerization partner) are shown for NEGR1 (green) and superimposed NTM (magenta), OBCAM (yellow), IGLON5 (blue-grey) and IGLON5 (pale green)/NEGR1 (olive). NEGR1 residues are labeled, as well as T^{64} in NTM. Residues that interact only via their main-chain atoms are shown as balls. NEGR1 residues that do not take part in the

interface, while their counterparts in other IgLONs do, are indicated with parentheses. A dashed circle indicates a region of high variability. See Table 2 for details. **e)** Same view as in **d)** but abstracting the information into three lines that correspond with residues forming the hydrophobic 'ridge' carrying the strictly conserved tryptophan and the 'hydrophobic pocket'. Residues that participate in ionic interactions are indicated. The tryptophan residue adopts multiple conformations in the different IgLONs; colors as in **d**) with the addition of NTM* in brown. The relative disposition of the Ig1 domains in representative IgLON structures as shown for the NEGR1, NTM, and OBCAM homodimers, respectively, whereby three dark-grey vertical lines represent an Ig1 domain (pale colors) orientated similarly to **d)** and three red lines represent the opposing Ig1 domain (darker colors) placed on top. **f)** Sequence conservation of NEGR1, NTM, OBCAM, LSAMP and IGLON5 mapped onto the Ig1 domain of NEGR1. Interface surface (left) and backside (right).

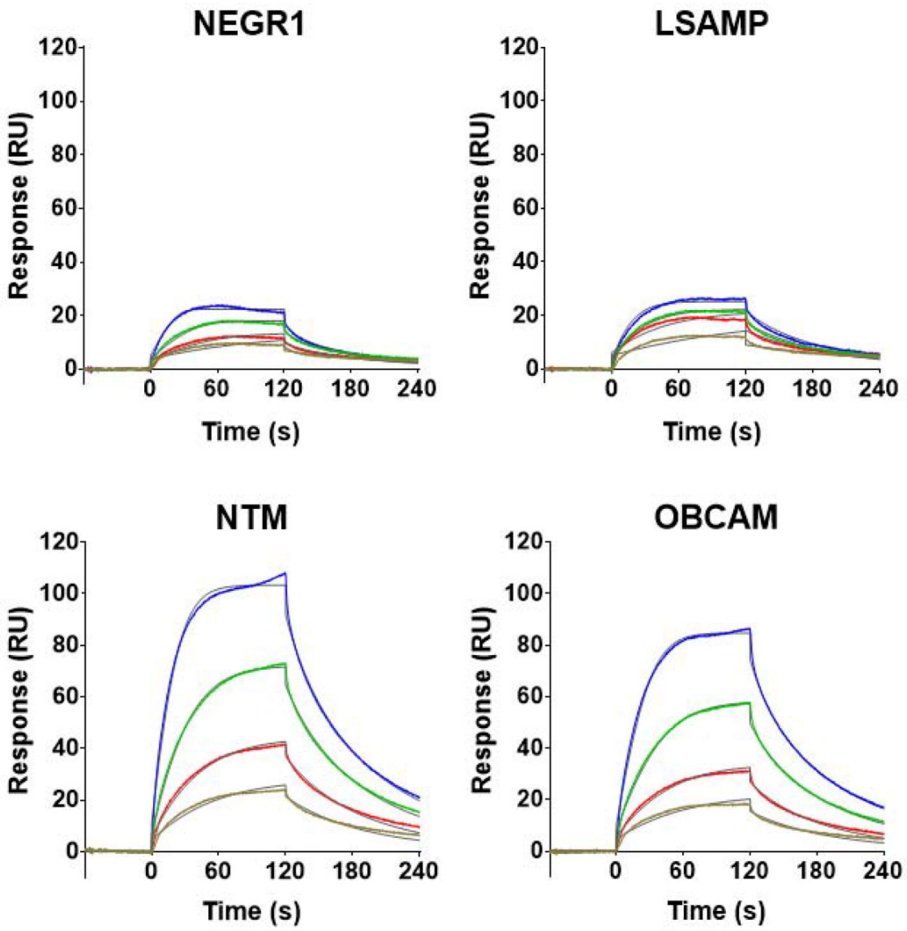

IgLON	K_D (nM)
NEGR1	21.3 ± 1.9
LSAMP	25.1 ± 0.4
NTM	30.1 ± 1.1
OBCAM	41.9 ± 1.2

Figure 6: Binding of NEGR1 to IgLON partners.

The binding of soluble IgLON ectodomains to a NEGR1-coupled CM5 sensor chip was monitored by SPR. Binding curves of the different IgLONs (0, 12.5, 25, 50 and 100 nM) in 10 mM HEPES pH 7.5, 150 mM NaCl, 0.05% (v/v) Surfactant P-20 were fit to a 1:1 binding model. **a)** NEGR1, **b)** LSAMP, **c)** NTM; **d)** OBCAM. The K_D values averaged over two experiments are shown together with the standard deviation.

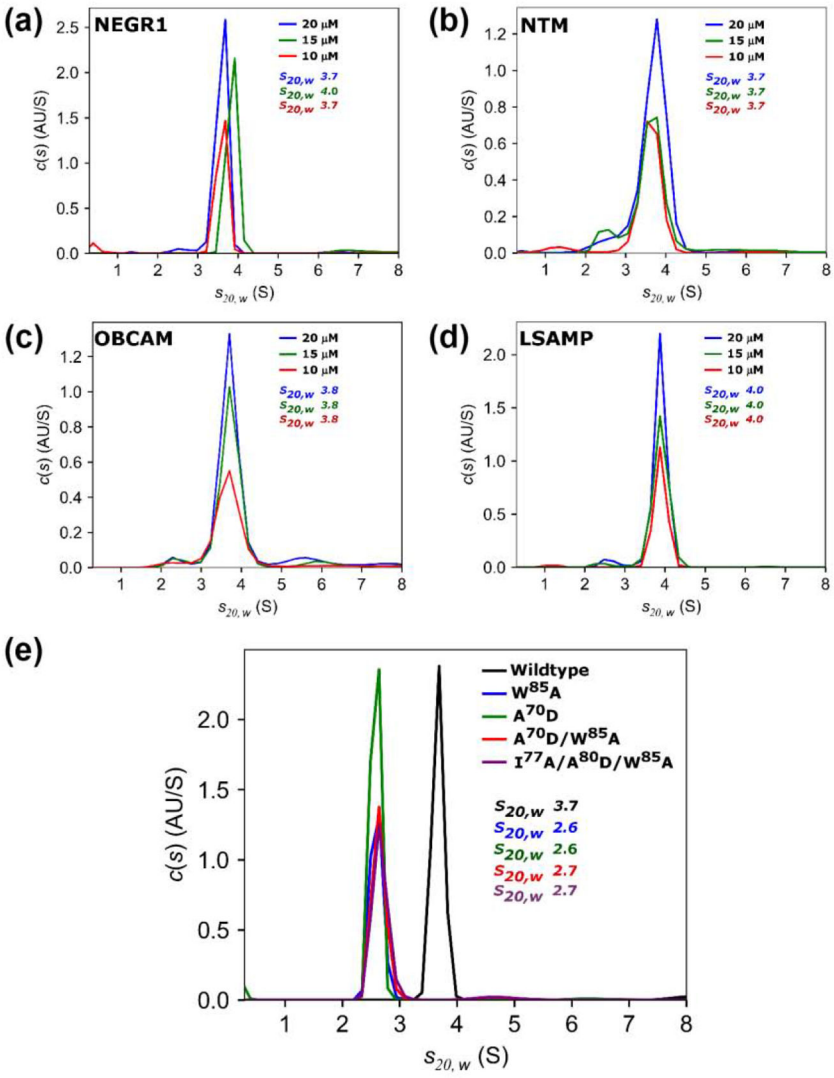

Mutant	Design strategy
NEGR1 $A^{70}D$	bury charge in the hydrophobic groove
NEGR1 $W^{85}A$	decrease the hydrophobic ridge size
NEGR1 $A^{70}D$, $W^{85}A$	alter hydrophobic ridge and groove
NEGR1 $I^{77}A$, $A^{80}D$, $W^{85}A$	alter hydrophobic ridge and groove

Figure 7: IgLON family members form dimers in solution.

Analytical ultracentrifugation sedimentation velocity analysis of **a)** NEGR1, **b)** NTM, **c)** OBCAM, **d)** LSAMP, and **e)** NEGR1 mutants $A^{70}D$, $W^{85}A$, $A^{70}D/W^{85}A$ and $I^{77}A/A^{80}D/W^{85}A$ designed to disrupt the Ig1-Ig1 dimerization interface compared to wild type NEGR1. The distribution of species $c(s)$ as a function of the experimental sedimentation coefficient 's_{exp}' was determined at 42,000 rpm (141,995 RCF) using three samples (10, 15, and 20 μM) for NEGR1, NTM, OBCAM, LSAMP, and 10 μM for the four NEGR1 mutants. The standardized s values $s_{20,w}$ (20 °C and water) are shown here. An $s_{20,w}$ ~3.7–4.0 corresponds to ~59–82 kDa (dimeric) and $s_{20,w}$ ~2.6–2.7 corresponds to ~30–37 kDa (monomeric) as calculated by SEDFIT.

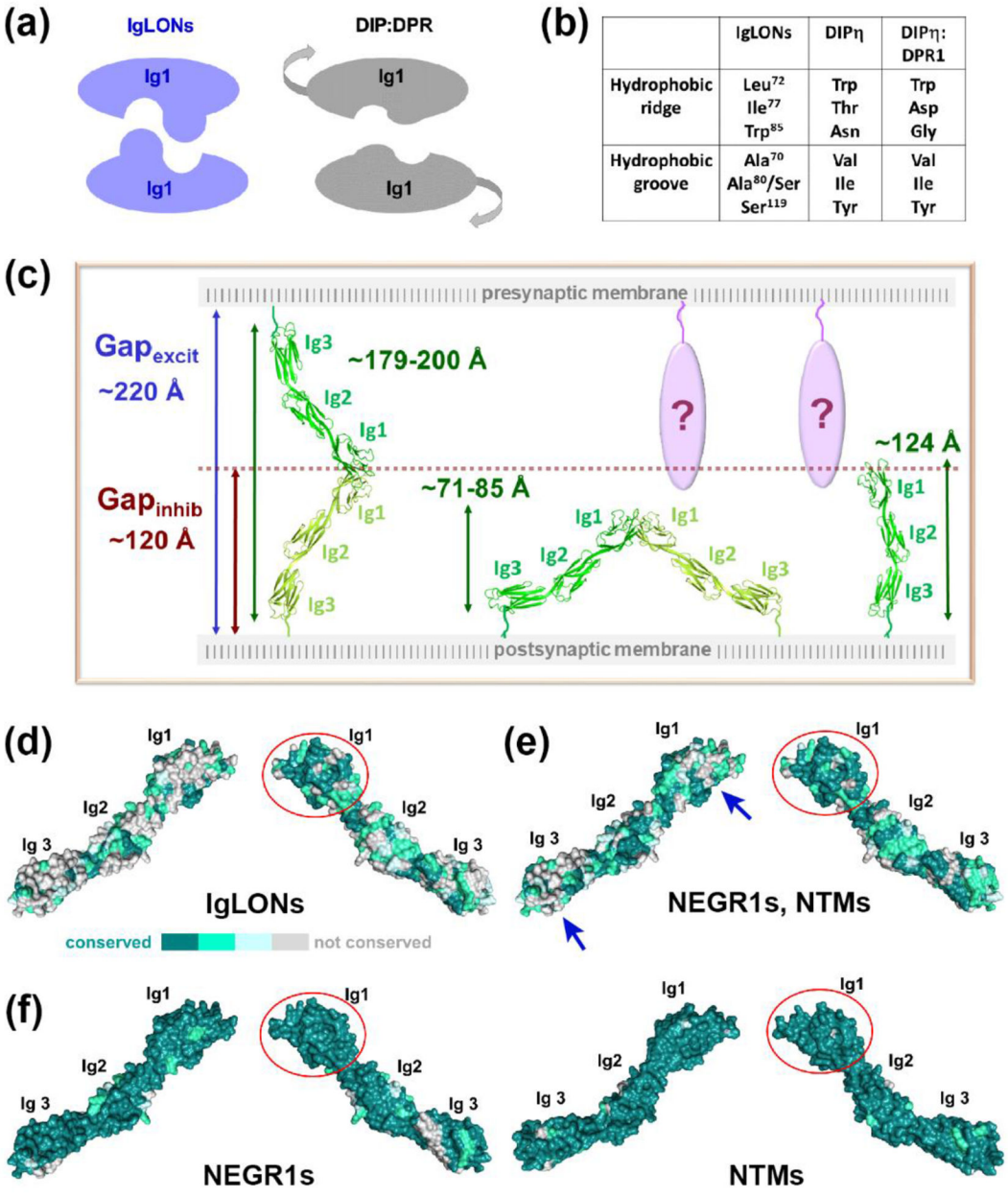

	IgLONs	DIPη	DIPη: DPR1
Hydrophobic ridge	Leu^{72} Ile^{77} Trp^{85}	Trp Thr Asn	Trp Asp Gly
Hydrophobic groove	Ala^{70} Ala^{80}/Ser Ser^{119}	Val Ile Tyr	Val Ile Tyr

Figure 8: Molecular mechanism of IgLONs.

a) Schematic of the interaction interface found in IgLONs and DIP/DPRs; **b)** Comparison of the conserved IgLON hydrophobic ridge and pocket with counterparts in DIPη homodimers and DIPη/DPR1 heterodimers; **c)** Possible configurations of IgLONs in the cleft of excitatory and inhibitory synapses, *trans*- dimers, *cis*- dimers and monomers. Putative non-IgLON protein partners shown in lilac; **d)** Sequence conservation of human NEGR1, NTM, OBCAM, LSAMP and IgLON5 mapped onto NEGR1; **e)** Sequence conservation between mammalian NEGR1s (10 sequences) and mammalian NTMs (10 sequences) mapped onto NEGR1. Strikingly divergent regions are marked with blue arrows; **f)** Sequence conservation

of mammalian NEGR1s (10 sequences) mapped onto NEGR1 (left) and mammalian NTMs (10 sequences) mapped onto NTM (right). In **d)** - **f)** the Ig1-Ig1 interface is encircled in red.

Table 1:

Data Collection and Refinement Statistics

	NEGR1	NTM
Data processing *		
Wavelength (Å)	1.00013	0.99999
Space group	$C222_1$	**$I4_1$**
Unit cell dimensions		
a, b, c (Å)	73.57, 97.24, 252.41	106.05, 106.05, 227.82
α, β, γ (°)	90, 90, 90	90, 90, 90
Resolution (Å)	31.81–3.01 (3.12–3.01)	46.43–3.32 (3.38–3.32)
Total reflections	126,270	83,262
Unique reflections	17,722 (715)	18,288 (817)
Completeness (%)	95.9 (77.0)	99.4 (93.4)
Multiplicity	7.1 (5.6)	4.6 (3.6)
Mean $I/\sigma(I)$	24.7 (1.9)	19.4 (1.0)
*R*merge (%)	7.6 (68.6)	7.3 (133.6)
*R*pim (%)	3.0 (28.7)	3.9 (78.0)
$CC_{1/2}$ (%)	87.9 (90.8)	98.4 (44.7)
Refinement *		
Resolution (Å)	31.81–3.01 (3.11–3.01)	46.43–3.32 (3.44–3.32)
Reflections used in refinement	14,290 (498)	15,247 (416)
Reflections used for R-free	499 (19)	504 (17)
R_{work} / R_{free} (%)	23.4 (31.7) / 28.6 (31.1)	22.96 (28.60) / 25.19 (23.49)
Total no. of non-hydrogen atoms	4,286	2,096
protein	4,168	2,017
carbohydrates	116	63
ions	2 (Ca^{2+})	3 (Cl^-)
others	-	12 (ethylene glycol)
Average B factor (Å^2)	56.9	72.9
protein (Å^2)	56.4	72.3
carbohydrates (Å^2)	76.1	94.3
ions (Å^2)	78.3	65.5
others (Å^2)	-	63.1 (ethylene glycol)
root mean square deviations		
bond lengths (Å)	0.002	0.002
bond angles (°)	0.48	0.56
Rotamer outliers (%)	0.0	0.0
Ramachandran plot residues		
favored (%)	95.0	94.8
allowed (%)	4.7	5.2
disallowed (%)	0.4	0.0

	NEGR1	NTM
MolProbity clash score	0.24	2.42
MolProbity overall score	0.94	1.38

* Numbers in parentheses refer to the highest-resolution shell

Table 2:

Residues mediating IgLON dimer formation based on currently available structures.

Cons.	NEGR1/ NEGR1	NEGR1/ IGLON5	NTM/NTM	NTM/ NTM*	OBCAM/ OBCAM	IgLON5/ IgLON5	IgLON5/ NEGR1	Notes
	reported here; PDB ID 6U6T	PDB ID 6DLD	reported here; PDB ID 6U7N	PDB ID 6DLF	PDB ID 5UV6	PDB ID 6DLE	PDB ID 6DLD	
	nse	nse	Thr^{64}	Thr^{64}	(Thr^{64})	(Thr^{61})	(Thr^{61})	
	Lys^{68}	Lys^{68}	Arg^{65}	Arg^{65}	Arg^{65}	Arg^{62}	Arg^{62}	WP; IA[a]
	Gly^{69}	Gly^{69}	Val^{66}	Val^{66}	Val^{66}	Val^{63}	Val^{63}	WP
*	Ala^{70}	Ala^{70}	Ala^{67}	Ala^{67}	Ala^{67}	Ala^{64}	Ala^{64}	WP
*	Leu^{72}	Leu^{72}	Leu^{69}	Leu^{69}	Leu^{69}	Leu^{66}	Leu^{66}	HR
*	(Arg^{74})	(Arg^{74})	(Arg^{71})	(Arg^{71})	Arg^{71}	(Arg^{68})	(Arg^{68})	
*	Ser^{75}	Ser^{75}	Ser^{72}	Ser^{72}	Ser^{72}	Ser^{69}	Ser^{69}	
	(Ser^{76})	Ser^{76}	Thr^{73}	Thr^{73}	Thr^{73}	Asn^{70}	Asn^{70}	
*	lie^{77}	lie^{77}	lie^{74}	lie^{74}	lie^{74}	Me^{71}	Me^{71}	HR
*	Ala^{80}	Ala^{80}	Ala^{77}	Ala^{77}	Ala^{77}	Ala^{74}	Ala^{74}	WP
*	Gly^{81}	Gly^{81}	Gly^{78}	(Gly^{78})	(Gly^{78})	(Gly^{75})	(Gly^{75})	WP
*	Asp^{83}	Asp^{83}	Asp^{80}	Asp^{80}	Asp^{80}	Asp^{77}	(Asp^{77})	IA[a]
	Lys^{84}	(Lys^{84})	Lys^{81}	Lys^{81}	Lys^{81}	Arg^{78}	Arg^{78}	
*	Trp^{85}	Trp^{85}	Trp^{82}	Trp^{82}	Trp^{82}	Trp^{79}	Trp^{79}	HR
	Ser^{86}	Ser^{86}	Cys^{83}	Cys^{83}	Ser^{83}	Thr80	Thr^{80}	
	Val^{87}	Val^{87}	Leu^{84}	Leu^{84}	lie^{84}	Ser^{81}	Ser^{81}	
*	(Asp^{88})	(Asp^{88})	Asp^{85}	(Asp^{85})	(Asp^{85})	(Asp^{82})	(Asp^{82})	
*	(Thr^{117})	Thr^{117}	Thr^{114}	Thr^{114}	Thr^{114}	Thr^{111}	Thr^{111}	HR
*	Ser^{119}	Ser^{119}	Ser^{116}	Ser^{116}	Ser^{116}	Ser^{113}	Ser^{113}	WP
	Val^{120}	(Val^{120})	Val^{117}	(Val^{117})	Val^{117}	Phe^{114}	(Phe^{114})	WP
	Gin^{121}	Gin^{121}	Gin^{118}	Gin^{118}	Gin^{118}	Gin^{115}	Gin^{115}	WP
*	Thr^{122}	(Thr^{122})	(Thr^{119})	Thr^{119}	Thr^{119}	Thr^{116}	(Thr^{116})	
	Gin^{123}	Gin^{123}	(Asp^{120})	(Asp^{120})	Asp^{120}	Arg^{117}	Arg^{117}	
	His^{124}	(His^{124})	Asn^{121}	(Asn^{121})	Asn^{121}	His^{118}	His^{118}	WP
	Thr^{125}	(Thr^{125})	(His^{122})	(His^{122})	His^{122}	Gin^{119}	(Gin^{119})	
*	Pro^{126}	Pro^{126}	Pro^{123}	Pro^{123}	Pro^{123}	Pro^{120}	Pro^{120}	WP
	(Arg^{127})	Arg^{127}	(Lys^{124})	(Lys^{124})	Lys^{124}	Tyr^{121}	Tyr^{121}	
*	(Thr^{128})	Thr^{128}	Thr^{125}	Thr^{125}	Thr^{125}	Thr^{122}	Thr^{122}	

Residues in the Ig1-Ig1 interface (within 5Å of the dimerization partner) are listed, aligned according to a structure-based sequence alignment [68]. Residues that are sequentially strictly conserved are indicated with '*'. Residues that are structurally conserved and establish interactions with the opposing Ig1 domain are listed without parentheses. Residues that are structurally conserved but do not establish interactions are in parentheses. Column "NEGR1/IgLON5" lists residues in NEGR1 interacting with IgLON5, while column "IgLON5/NEGR1" lists residues in IgLON5

interacting with NEGR1. Cons., sequence conservation; HR, hydrophobic ridge; IA, ionic interaction; nse, no structurally equivalent residue present; WP, tryptophan pocket.

[a] ionic interaction not established in the NTM homodimer.